Liquid Crystals
Publication details, including instructions for authors and subscription information:
http://www.informaworld.com/smpp/title~content=t713926090

New chlorine-substituted liquid crystals possessing frustrated TGB_A and SmQ phases

Miroslav Kašpar[a]; Petra Bílková[a]; Alexej Bubnov[a]; Věra Hamplová[a]; Vladimíra Novotná[a]; Milada Glogarová[a]; Karel Knížek[a]; Damian Pociecha[b]
[a] Institute of Physics, Academy of Sciences of the Czech Republic, 182 21 Prague 8, Czech Republic [b] Laboratory of Dielectrics and Magnetics, Chemistry Department, Warsaw University, 02-089 Warsaw, Poland

To cite this Article Kašpar, Miroslav , Bílková, Petra , Bubnov, Alexej , Hamplová, Věra , Novotná, Vladimíra , Glogarová, Milada , Knížek, Karel and Pociecha, Damian(2008) 'New chlorine-substituted liquid crystals possessing frustrated TGB_A and SmQ phases', Liquid Crystals, 35: 5, 641 — 651
To link to this Article: DOI: 10.1080/02678290802056212
URL: http://dx.doi.org/10.1080/02678290802056212

Liquid Crystals,
Vol. 35, No. 5, May 2008, 641–651

Taylor & Francis
Taylor & Francis Group

New chlorine-substituted liquid crystals possessing frustrated TGB_A and SmQ phases

Miroslav Kašpar[a], Petra Bílková[a]*, Alexej Bubnov[a], Věra Hamplová[a], Vladimíra Novotná[a], Milada Glogarová[a], Karel Knížek[a] and Damian Pociecha[b]

[a]*Institute of Physics, Academy of Sciences of the Czech Republic, Na Slovance 2, 182 21 Prague 8, Czech Republic;* [b]*Laboratory of Dielectrics and Magnetics, Chemistry Department, Warsaw University, Al. Zwirki i Wigury 101, 02-089 Warsaw, Poland*

(Received 16 August 2007; final form 14 March 2008)

Several series of chlorine-substituted rod-like liquid crystalline compounds have been synthesised containing a different number of lactate units in the chiral chain. Sequences of phases and phase transition temperatures were determined by differential scanning calorimetry, polarising optical microscopy and X-ray diffraction studies. Depending on the molecule structure, the materials possess a rich variety of mesophases, i.e. the paraelectric chiral smectic A (SmA*), ferroelectric chiral smectic C (SmC*) and antiferroelectric smectic C (SmC_A*) phases. Additionally, some compounds with one and two lactate groups exhibit the frustrated antiferroelectric twist grain boundary (TGB_A) and smectic Q (SmQ) phases, respectively. The existence of the SmQ phase ordered in two directions was confirmed by X-ray diffraction on a non-oriented sample. The effects of the non-chiral chain length and number of the chiral lactate groups on the mesomorphic properties, spontaneous polarisation, spontaneous tilt angle and complex permittivity have been studied and discussed.

Keywords: chiral liquid crystal; lactate group; chlorine substitution; ferroelectric smectic phase; twist grain boundary phase; SmQ phase; spontaneous polarisation; dielectric properties

1. Introduction

Recently, it has been found that materials with three phenyl rings in their molecular core and a chiral part based on the lactate unit possess a ferroelectric chiral smectic C (SmC*) phase (*1–3*) and, in the case of two lactate units, a tendency to form the antiferroelectric chiral smectic C (SmC_A*) phase has been discovered (*2, 4*). A rare re-entrant ferroelectric phase and the ferroelectric hexatic phase have been found in some of these materials (*4*). Additionally, the presence of the second and third lactate units in such a molecule leads to a decrease of the phase transition temperatures in comparison with an analogous molecule with only one lactate group (*2, 3*).

A very broad SmC* phase was found in materials with a molecular core possessing one biphenyl moiety substituted by chlorine, two more aromatic rings connected by the ester linkage and a chiral part containing one lactate group (*5*). Non-substituted materials possessing four aromatic rings in their molecular core exhibit extremely high clearing temperatures resulting in material decomposition when approaching the isotropic phase. However, the lateral substitution by the chlorine atom has been suggested as an efficient tool for decreasing the phase transition temperatures (*6, 7*).

In chiral liquid crystalline systems, a variety of frustrated phases can occur and have been reported (*8, 9*). Twist grain boundary (TGB) phases, which form as a result of the competition between stabilisation of the smectic layered structure and the tendency of molecules to form a helicoidal structure, and blue phases with a cubic structure (*10, 11*) are examples of frustrated mesophases. The existence of the TGB phase was predicted by Renn and Lubensky (*12*). Renn (*13*) suggested three different types of TGB phases in which the local ordering is like in the chiral smectic A (SmA*), SmC and SmC* phases. The antiferroelectric twist grain boundary (TGB_A) phase was discovered by Goodby *et al.* in the phenyl propiolates (*14–16*). Nevertheless, the relationship between the molecular structure and formation of the TGB phases is still unknown and a systematic study of physical properties is difficult because of a narrow temperature interval of their existence. Presence of a frustrated phase is connected with the high twisting power.

Another frustrated phase existing between the antiferroelectric SmC_A* and isotropic phases is the smectic Q (SmQ) phase (*8, 17–20*). This phase was first reported by Levelut *et al.* (*18*) and has so far been observed somewhat rarely. A similar frustrated structure (*9*) was found in some dichiral mesogens, where the chirality was a dominant factor to form the cubic superstructure (*21, 22*). Location of the chiral moieties in the molecular structure seems to have a significant effect on the appearance of these chirality-induced frustrated superstructures. The SmQ phase has been reported in materials possessing the identical

*Corresponding author. Email: bilkova@fzu.cz

ISSN 0267-8292 print/ISSN 1366-5855 online

DOI: 10.1080/02678290802056212
http://www.informaworld.com

chiral moiety at both sides of the rigid molecular core (*9, 17–20*). X-ray studies of the SmQ phase enable identification of four different structure types all belonging to the class of defect crystals (*18*). Two of them can be described as an array of twist boundaries in antiferroelectric smectics (*19*). One of these four structures concurs with $I4_122$ symmetry (*18, 23*). Two different models designated as I and II have been proposed (*23*) to interpret the architecture of the SmQ phase with $I4_122$ symmetry. Both model structures are built from elementary blocks composed of pieces of the SmC_A* double-layers with differing orientation of molecules. Model I should exhibit much lower birefringence than model II (*23*).

Chlorine substitution serves as a promising tool to enlarge the polarisation, as it was confirmed previously. Additionally, such a substitution can lead to a lowering of the clearing temperature (*15*). We have focused on new series of materials having two biphenyl moieties in their molecular core with chlorine substitution. Recently, a series of mesogens with four phenyl rings in their molecular core have been presented (*5*). The molecular structure contains one flexible ester group connecting two phenyls and one biphenyl substituted in the ortho-position to the *n*-alkoxy chain. All such compounds exhibit very broad temperature intervals of the SmA* and SmC* phases, which can reach up to 200 K. In spite of an effective lowering of the clearing point in comparison with non-substituted compounds (*5*), all mesogens exhibit still relatively high transition temperatures. We intended to remove the ester group and prepare a more rigid molecular core, which could diminish the transition temperatures. Multiple lactates have been used to increase the probability of the occurrence of an antiferroelectric phase (*2–4*). Taking into account the above-mentioned knowledge, three series with one, two or three lactate units in the chiral part and with a varying length of the non-chiral chain have been synthesised. Their mesomorphic properties have been studied and compared for different number of lactate groups. The chirality-induced frustrated phases between the isotropic melt and the ordinary smectic phases have been observed and their behaviour discussed. The results contribute to an understanding of the relationship between molecular structure and the formation and properties of ferroelectric, antiferroelectric and frustrated liquid crystal phases.

2. Synthesis

Several series of materials possessing one, two and three chiral lactate units, differing in the length of the non-chiral chain, have been synthesised. A general chemical formula is shown in Scheme 1.

The synthetic procedure was carried out according to Scheme 2.

The synthesis of chiral alcohols **1a–1c** (see Scheme 2) has been described in detail elsewhere (*1*). All the chiral centres have an (*S*) configuration.

Phenols **2a–2c** were synthesised in the following way. Chiral alcohols **1a–1c** were esterified by protected 4-hydroxy-4′-biphenylcarbonyl chloride in a pyridine/dichloromethane mixture followed by ammonolysis in chloroform/tetrahydrofuran mixture at a temperature of 10°C. After separation of the reaction mixture by column chromatography on the silica gel (using a mixture 99:1 of dichloromethane and acetone as the eluent), materials **2a–2c** were obtained in 50% yield. Molecular structures of materials were checked by ^{1}H NMR (200 MHz, $CDCl_3$, Varian, Gemini 2000). Preparation of the 4-alkoxy-3-chloro-4′-biphenylcarboxylic acids (**3**) was described in our previous work (*5*).

Final materials **1Ln, 2Ln** and **3L5** were prepared by standard methods of esterification with dicyclohexylcarbodiimide (DCC) in the presence of dimethylaminopyridine (DMAP) in dichloromethane. Crude products were purified by column chromatography on silica gel using a mixture (99.5:0.5) of dichloromethane and acetone as an eluent and crystallised twice from acetone. Structures of all final products were confirmed by ^{1}H NMR (200 MHz, $CDCl_3$, Varian, Gemini 2000). Chemical purity of materials was checked by high-performance liquid chromatography (HPLC), which was carried out with an Ecom HPLC chromatograph using a silica gel column (Separon 7 μm, 3 × 150, Tessek) with a mixture of 99.8% of toluene and 0.2% of methanol as an eluent. Eluting products were detected by a spectrophotometric UV–visible detector (λ=290 nm). The chemical purity was found better than 99.8% under these conditions.

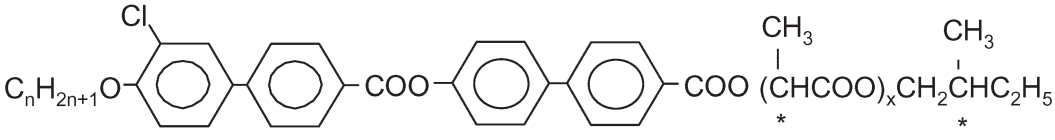

Scheme 1. Chemical formula of the studied materials; *n*, the number of carbon atoms in the non-chiral chain, varies from 5 to 13. According to the number of lactate units (x=1, 2, 3), materials are denoted as **xLn** and divided into three series.

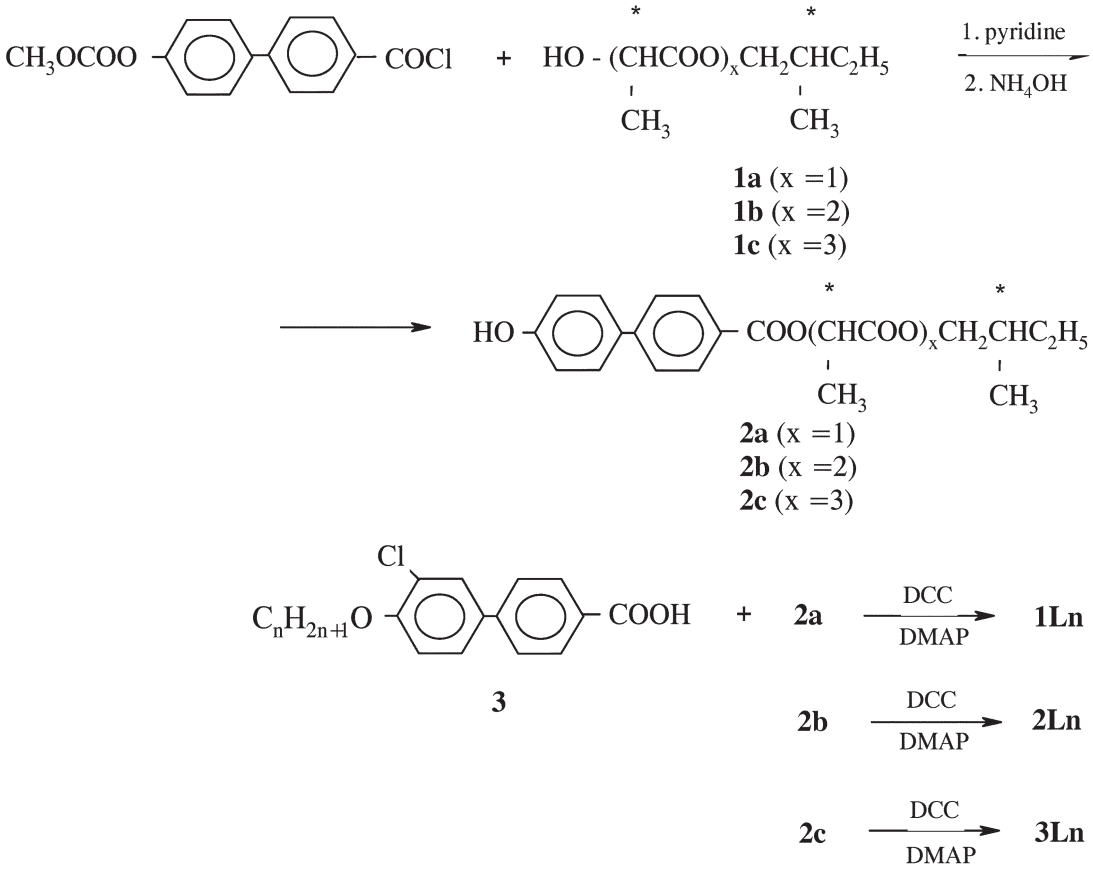

Scheme 2. Synthetic procedure for preparation of the new liquid crystalline compounds.

^{1}H NMR ($CDCl_3$, 200 MHz) for **2b**: 8.10d (2H, ortho to –COO); 7.58d (2H, meta to –COO); 7.42d (2H, meta to –OH); 6.90d (2H, ortho to –OH); 5.40q (1H, ArCOOCH*); 5.20q (1H, C*COOCH*); 4.00m (2H, $COOCH_2$); 1.60 and 1.75d+d (6H, CH_3CHCOO); 1.20–1.70m (3H, $CHCH_2$); 0.90t (3H, CH_3).

^{1}H NMR ($CDCl_3$, 200 MHz) for **2L8**: 8.28d (2H, ortho to –COOAr); 8.18d (2H, ortho to –COOC*); 7.70m (7H, ortho to –Ar); 7.52dd (1H, para to –Cl); 7.38d (2H ortho to –OCOAr); 7.02d (1H, meta to –Cl); 5.40q (1H, ArCOOCH*); 5.22q (1H, C*COOCH*); 4.00–4.10m (4H, CH_2OAr and $COOCH_2$); 1.60 and 1.78d+d (6H, CH_3CH^*COO); 1.20–1.90m (15H, $CH+CH_2$); 0.90t (6H, CH_3).

3. Experimental results

Study of characteristic textures and their changes as well as the measurements of the spontaneous polarisation and tilt angle were carried out on planar samples in the bookshelf geometry, filled in the isotropic phase into 25 μm thick glass cells by means of capillary action. The inner surfaces of the glass plates were covered by ITO electrodes. The sample thickness was defined by mylar sheets. Improvement of uniform planar alignment, required especially for measurements of the tilt angle, has been reached by application of electric field (10–20 Hz, 40 kV cm^{-1}) applied for 5–30 min. Free-standing films (FSFs) providing homeotropic alignment due to the air–liquid crystal interface were prepared by manual spreading of the melted compound over a circular hole (3 mm) in a metal plate.

The sequence of the phases and their phase transition temperatures were determined from characteristic textures and their changes observed on the planar cells as well as on the free-standing films in polarising optical microscope (Nikon Eclipse E600POL). A Linkam LTS E350 heating stage with TMS 93 temperature programmer was used for the temperature control, which enabled the temperature stabilisation within ± 0.1 K. The phase transition temperatures were checked by a differential scanning calorimetry (DSC) yielding also the transition enthalpies. The DSC measurements were carried out with Pyris Diamond Perkin-Elmer 7 on cooling and heating runs at a rate of 5 K min^{-1}. For DSC measurements the sample (2–6 mg) was hermetically sealed in an aluminium pan and placed in nitrogen atmosphere.

Values of the spontaneous polarisation, P_s, were evaluated from the *P(E)* hysteresis loop detected during P_s switching in an ac electric field, E, of frequency 50 Hz. Values of the spontaneous tilt angle, θ_s, were determined optically from the difference between extinction positions under crossed polarisers under opposite dc electric fields $\pm 40\,\mathrm{kV\,cm^{-1}}$. Well-aligned samples were used for θ_s measurements.

Several materials were studied by the small-angle diffraction technique. The layer spacing, d, was determined using a modified DRON system equipped with a Cu tube and a graphite monochromator. Experiments were conducted in the reflection mode for a non-oriented sample with one free surface. Sample temperature was controlled within 0.1 K. The heating/cooling rate was $1\,\mathrm{K\,min^{-1}}$. The layer spacing d was determined using the Bragg law:

$$n\lambda = 2d\sin\Theta. \quad (1)$$

The structure of the **2L13** material was studied using an X-ray powder diffractometer (Bruker D8, Cu K_α, SOL-X energy dispersive detector) equipped with wide range temperature chamber.

The frequency dispersion of the complex permittivity, $\varepsilon^*(f)=\varepsilon'-\mathrm{i}\varepsilon''$, was measured using a Schlumberger 1260 impedance analyser in the frequency range 1 Hz–10 MHz keeping the temperature of the sample stable within ± 0.1 K during the frequency sweep. The frequency dispersion data were analysed using the Cole–Cole formula for the frequency dependent permittivity complemented by the second and third terms with the aim to eliminate a low frequency contribution to ε'' from dc conductivity, σ, and the high-frequency contribution due to the resistance of the ITO electrodes, respectively:

$$\varepsilon^* - \varepsilon_\infty = \frac{\Delta\varepsilon}{1+(\mathrm{i}f/f_r)^{(1-\alpha)}} - \mathrm{i}\frac{\sigma}{2\pi\varepsilon_0 f^n} + Af^m, \quad (2)$$

where f_r is the relaxation frequency, $\Delta\varepsilon$ is the dielectric strength, α is the distribution parameter of the relaxation times and *n, m, A* are fitting parameters.

Mesomorphic properties

Mesomorphic properties of the new materials were studied by polarising optical microscopy and DSC. Results of these studies for materials with one, two and three lactate units are presented in Tables 1, 2 and 3, respectively. Some of the phase transitions were clearly seen under the microscope as change of texture but were not accompanied by a peak in the DSC plot. In Figures 1(a) and 1(b), phase transition diagrams are presented for the homologues series **1Ln** and **2Ln**, respectively.

All studied compounds from the **1Ln** series exhibit a SmC* phase. In addition, homologues with a short non-chiral chain (n=5–8) exhibit broad temperature range of the paraelectric SmA* phase; the homologues with n=9 and 10 possess the TGB_A instead of the SmA* phase. For materials with n=11 and 12, a direct transition between the isotropic and the SmC* phases occurs (see Figure 1(a)).

The TGB_A phase has been identified according to typical blurred coloured textures (*24*) obtained in planar samples (see Figure 2(a) for **1L9**). Moreover, this phase does not switch under an applied electric field of the opposite polarity and the values of the real part (ε') of the complex permittivity are lower than those typical for the SmC* phase. In the FSF films, a characteristic filament texture was observed for films a few μm thick (see Figure 2(b) for **1L9**). Such a texture has been commonly found in the TGB_A phase in samples with the homeotropic surface alignment (*24*). It was supposed that filaments were TGB_A phase areas embedded in the homeotropic SmA* phase, resulting from the TGB_A phase by the action of the surface anchoring. For a FSF about 10 μm thick we found a stripe texture in the TGB_A phase, which has not been observed previously (Figure 2(c)). We suggest that the stripes represent

Table 1. The sequence of phases, the phase transition temperatures (°C) and the phase transition enthalpies ΔH ($\mathrm{J\,g^{-1}}$) measured on cooling and the melting points, m.p. (°C), measured on heating by DSC ($5\,\mathrm{K\,min^{-1}}$) for the **1Ln** series. The symbols "•" and "–" show that the phase exists or does not exist, respectively. (msc – the phase transition temperature was determined from microscope observations).

	m.p.	Cr_2		Cr_1		SmC*		SmA*		TGB_A		I
1L5	113 [+36.7]	•	36 [−8.9]	•	52 [−1.1]	•	130 [−0.5]	•	203 [−3.8]	–		•
1L6	100 [+31.5]	–		•	31 (msc)	•	136 [−0.2]	•	198 [−3.2]	–		•
1L7	93 [+30.7]	–		•	38 (msc)	•	145 [−0.7]	•	195 (msc)	–		•
1L8	89 [+26.9]	–		•	24 [−3.8]	•	160 [−0.5]	•	193 (msc)	–		•
1L9	82 [+22.8]	–		•	4 [−0.1]	•	154 [−0.5]	–		•	176 (msc)	•
1L10	74 [+19.1]	–		•	39 [−9.8]	•	161 [−0.6]	–		•	164 [−0.2]	•
1L11	74 [+21.3]	•	7 [−0.05]	•	39 [−0.4]	•	156 (msc)	–		–		•
1L12	86 [+16.7]	•	40 [−10.5]	•	74 [−21.3]	•	159 [−1.4]	–		–		•

Table 2. The sequence of phases, the phase transition temperatures (°C) and the phase transition enthalpies ΔH ($J\,g^{-1}$) measured on cooling and the melting points, m.p. (°C), measured on heating by DSC ($5\,K\,min^{-1}$) for the **2Ln** series. The symbols "•" and "–" show that the phase exists or does not exist, respectively. (msc – the phase transition temperature was determined from microscope observations).

	m.p.	Cr		SmC_A*		SmC*		SmA*		SmQ		I
2L5	134 [+48.2]	•	75 [−29.1]	•	107 [−0.1]	•	114 [−0.1]	•	191 [−3.8]	–		•
2L6	131 [+46.9]	•	80 [−31.6]	•	109 [−0.2]	•	121 [−0.1]	•	183 [−2.6]	–		•
2L7	123 [+40.9]	•	80 [−27.7]	•	115 [−0.1]	•	132 [−0.3]	•	162 [−0.9]	–		•
2L8	108 [+35.8]	•	62 [−22.5]	•	119 [−0.2]	•	133 [−0.8]	–		–		•
2L9	97 [+28.6]	•	60 [−19.7]	•	103 [−0.6]	–		–		–		•
2L10	93 [+27.5]	•	62 [−20.4]	•	103 [−1.1]	–		–		–		•
2L11	91 [+23.7]	•	65 [−18.4]	•	108 [−0.4]	–		–		•	108 [−0.5]	•
2L12	92 [+22.7]	•	67 [−22.0]	•	94 (msc)	–		–		•	111 [−0.4]	•
2L13	86 [+16.7]	•	60 [−16.0]	•	91 (msc)	–		–		•	114 [−0.4]	•

Table 3. The sequence of phases, the phase transition temperatures (°C) and the phase transition enthalpies ΔH ($J\,g^{-1}$) measured on cooling and the melting point, m.p. (°C), measured on heating by DSC ($5\,K\,min^{-1}$) for compound **3L5**. The symbols "•" show that the phase exists. (msc – the phase transition temperature was determined from the microscope observation).

	m.p.	Cr_2		Cr_1		SmC*		SmA*		Iso
3L5	120 [+31.0]	•	63 [−2.8]	•	72 [−7.7]	•	108 (msc)	•	183 [−3.1]	•

blocks of the SmA* phase with the smectic layers slightly inclined from the horizontal orientation and separated by defects. Because of surface tension the TGB helix could not be fully developed.

In the SmC* phase, the typical schlieren texture was observed in the FSF of all studied compounds, reflecting distortion of the director field due to degeneration of the direction of the molecular tilt. The colours are caused by selective reflection in the range of the visible light due to a rather small value of the pitch.

All studied homologues from **2Ln** series with two lactate units exhibit the SmC_A* phase (see Table 2), which is monotropic for the compounds with the short non-chiral chains (n=5–7). The same homologues possess the SmA* and the SmC* phases. For compound **2L8,** a direct phase transition from the isotropic to the SmC* phase is observed. For compounds with n=11–13, a mosaic texture is observed in the planar sample just below the isotropic phase (see Figure 3(a)). This peculiar texture resembles the one specific to the SmQ phase (*8, 23*). The assignment of this texture to the SmQ phase is qualified below by the X-ray diffraction studies. The microphotograph of the SmQ texture obtained in the FSF is shown in Figure 3(b). This is the first presented FSF texture in the SmQ phase. A low-birefringent texture with a mosaic or stripe character of textural features has been created by a very slow cooling from the isotropic phase (at least $0.5\,K\,min^{-1}$). Approaching the antiferroelectric phase on the subsequent cooling, the contrast gradually grows. Rotating the sample towards the crossed polariser and analyser, the domains could be turned to the extinction position. A strong temperature hysteresis was observed in the occurrence of both the isotropic and the SmQ phases. This hysteresis is clearly seen in the DSC plot for **2L13** compound shown in Figure 4. Moreover, the SmQ phases persists in coexistence with the SmC_A* phase on cooling, as was confirmed by the X-ray study described below. The width of the temperature interval of this coexistence strongly depends on the cooling rate. The transition from the SmQ to the SmC_A* phase takes about 60 min to fully develop. If the cooling process is not stopped at the beginning of this transition, the SmQ phase coexists with the SmC_A* phase down to crystallisation. The mesomorphic behaviour of **2L11** and **2L12** is very similar.

Only one homologue with three lactate units, **3L5**, has been synthesised, exhibiting the SmA* and the SmC* phases on cooling over a broad temperature ranges. The SmC* phase is fully monotropic, the melting point being within the temperature range of the SmA* phase (see Table 3). Due to very low value of enthalpy (lower than $0.1\,J\,g^{-1}$), the SmA*–SmC* phase transition could not be detected by DSC.

All studied materials exhibit the relatively high values of the melting point. In the monotropic ranges of the SmC* and SmC_A* phases the electric field can cause the crystallisation. For some compounds from **1Ln** series as well as for **3L5**, a crystal–crystal phase transition was detected. The crystal phases of different structures are denoted as Cr_1 and Cr_2 (see Tables 1 and 3).

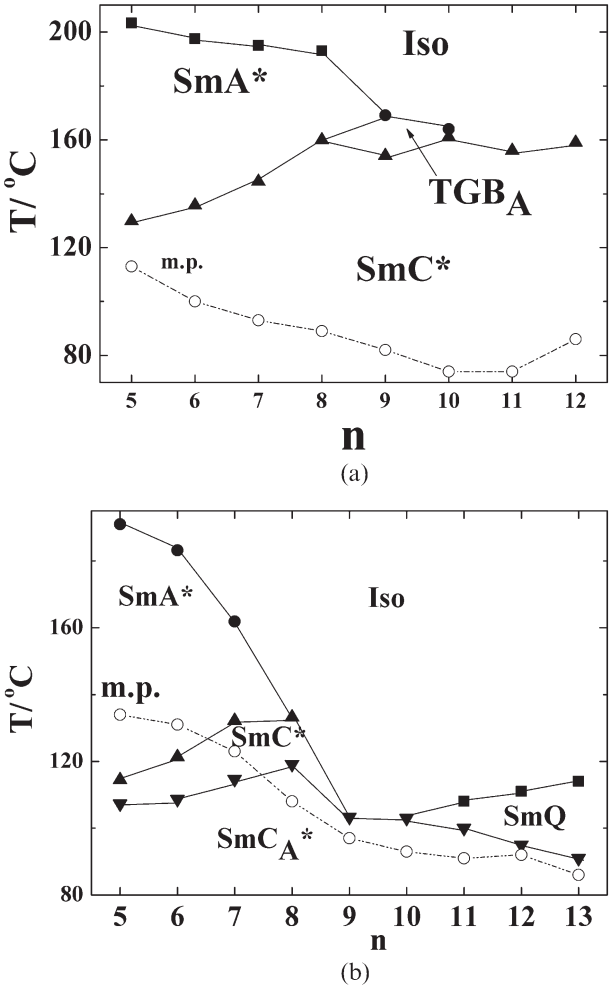

Figure 1. Phase transition diagrams of series (a) **1Ln** and (b) **2Ln**. The phases are indicated; "open" symbols show the melting points (m.p.). To reach the SmQ phase (**2Ln** series) a very slow cooling has to be applied with a rate less than 0.1 K min^{-1}.

X-ray scattering results

Small-angle X-ray scattering studies were performed for the **2L13** homologue in the temperature range ascribed to the SmQ phase. The intensity of the scattered beam versus diffraction angle, 2Θ, is shown in Figure 5. In the temperature range of the SmQ phase, two peaks have been detected, indicating a layered structure modulated in two directions with corresponding periodicities of 37.6 Å and 33.0 Å for 200 and 004 reflection, respectively, assuming $I4_122$ symmetry. In the temperature range of the SmQ and SmC$_A$* phase coexistence, a strong additional peak corresponding to the layer spacing of the SmC$_A$* phase is seen.

In the smectic phases, the layer spacing, d, evaluated using the Bragg law [equation (1)] is presented in Figure 6 for three selected compounds ***x*L5** (x=1, 2, 3). In the orthogonal SmA* phase, d is nearly temperature independent. The decrease of d below the phase

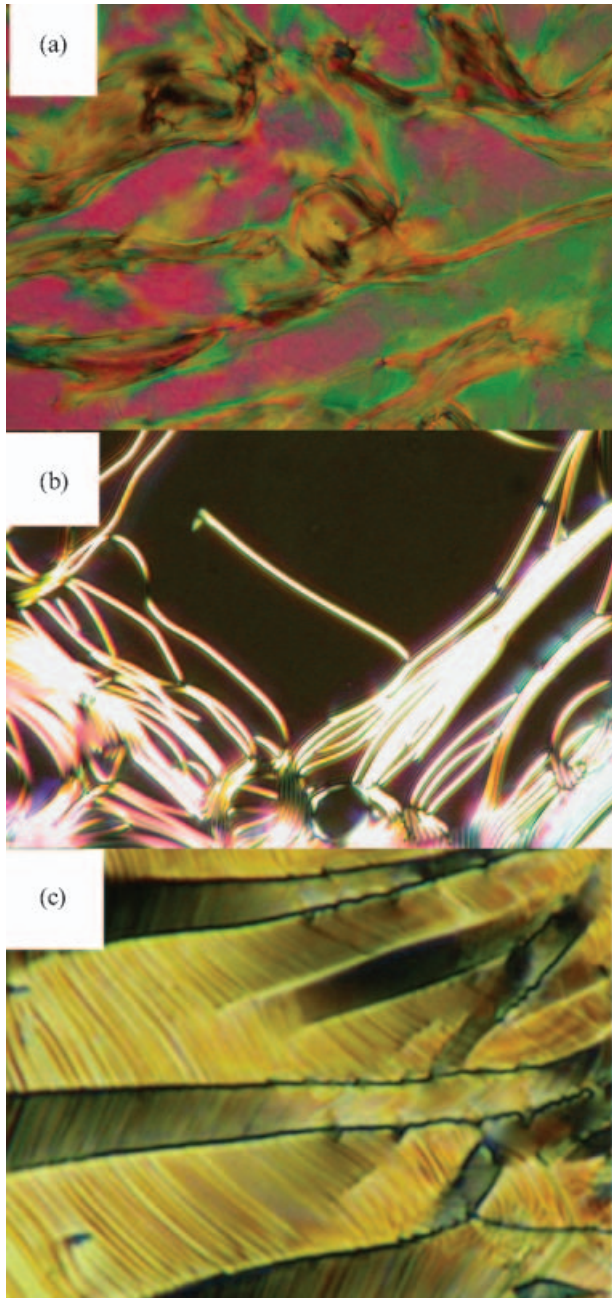

Figure 2. Microphotographs of textures in the TGB$_A$ phase of **1L9** obtained on cooling from the isotropic phase: (a) planar sample at 168°C; (b) thin free-standing film at about 163°C; (c) free-standing film of thickness more than 10 µm at about 164°C.

transition to the SmC* phase is a consequence of the molecule tilt in the SmC* phase and d continues to decrease within the SmC$_A$* phase.

Spontaneous polarisation and tilt angle

The temperature dependences of the spontaneous polarisation, P_s, and spontaneous tilt angle, θ_s, were

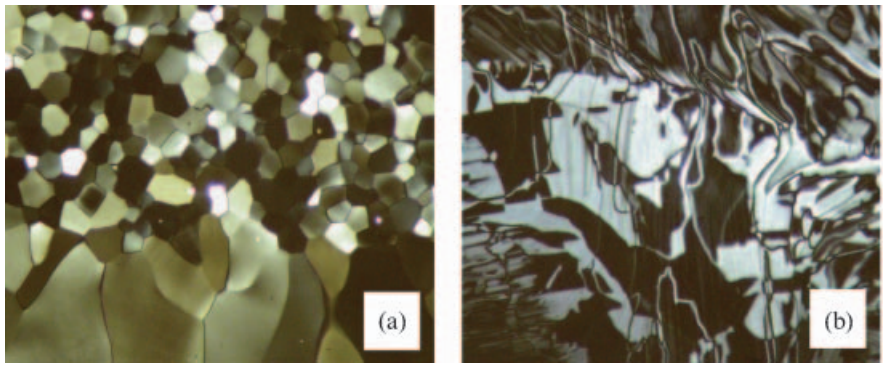

Figure 3. Microphotographs of textures in the SmQ phase of **2L13** obtained (a) for a planar sample at 118°C and (b) in free-standing film at 100°C. The textures were developed on very slow heating.

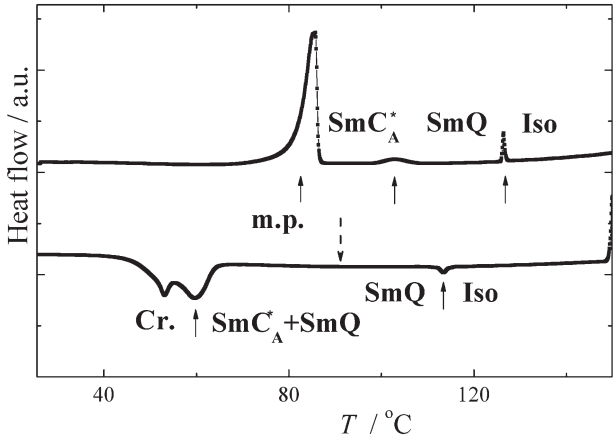

Figure 4. DSC plots for heating and cooling runs ($5\,K\,min^{-1}$) of compound **2L13**. Solid arrows indicate the phase transitions. The dashed arrow shows the temperature where the SmC_A* phase started to appear, as determined by microscopic observation. The phase coexistence region is indicated as SmQ + SmC_A*. The second peak below the crystallisation shows a phase transition in the crystal phase with different structure.

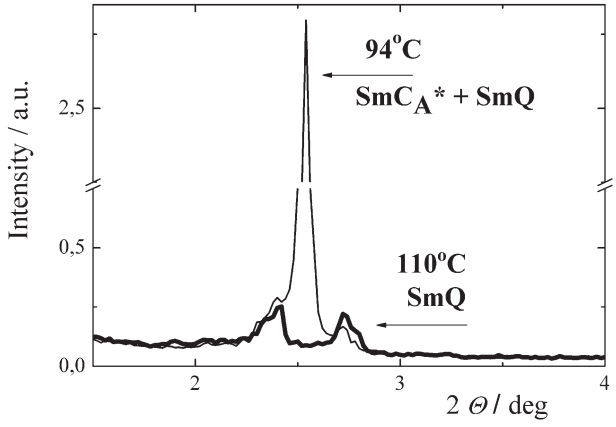

Figure 5. The X-ray intensity profile versus the scattering angle 2Θ taken on **2L13** compound presented for two distinct temperatures on cooling from isotropic phase. The "thick" line corresponds to the indicated temperature T=110°C in the SmQ phase, the "thin" line to T=98°C, where the SmQ and SmC_A* coexist.

measured in the SmC* and SmC_A* phases. The results are shown in Figures 7 and 8 for the indicated compounds from **1Ln** and **2Ln** series, respectively. In the temperature ranges of these phases located below the melting point, the electric field applied during $P_s(T)$ and $\theta_s(T)$ measurements stimulates the crystallisation, which makes it impossible to measure these quantities in the whole temperature range of the field-free phase existence (see Table 1).

For the **1Ln** and **2Ln** series, both P_s and θ_s exhibit a discontinuity at the SmA*–SmC* phase transition, suggesting a first-order transition except for the compounds with the shortest non-chiral molecular chain (n=5, 6), the discontinuity increasing with increasing n (see Figures 7–8). The P_s as well as θ_s values are relatively high. Generally, both are higher for the **1Ln** series. In this series, θ_s values reach nearly

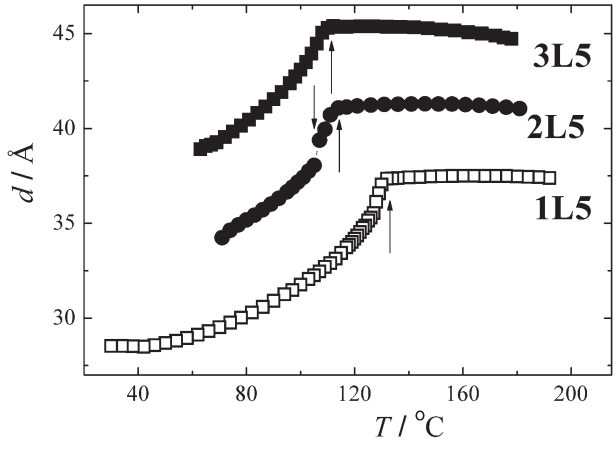

Figure 6. The temperature dependence of the layer spacing for ***x*L5** compounds, x=1, 2, 3. The up arrows indicate the phase transition to the SmC* phase; the down arrow indicates the phase transition to the SmC_A* phase.

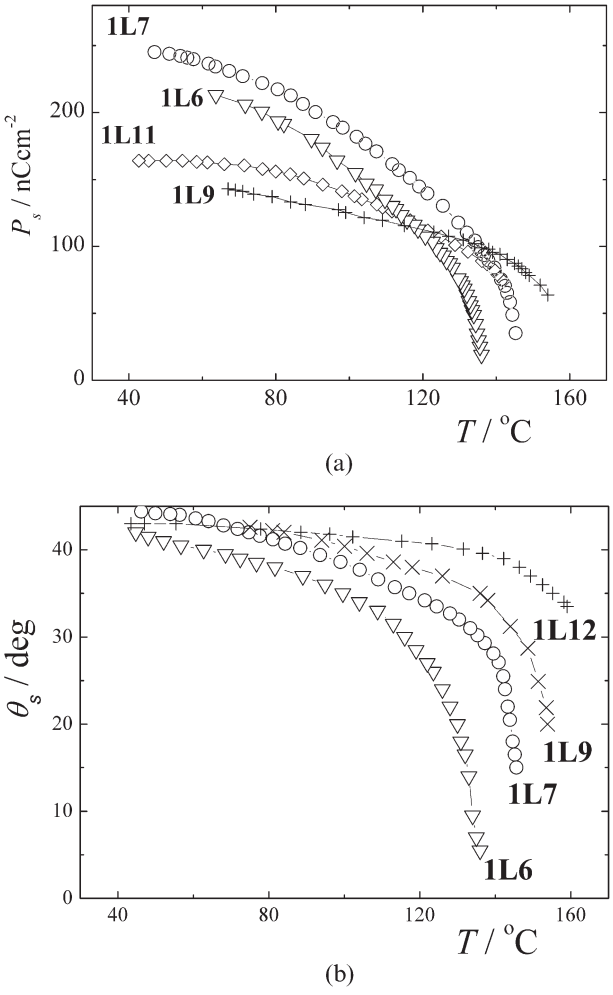

Figure 7. The temperature dependence of (a) the spontaneous polarisation and (b) the spontaneous tilt angle for indicated **1Ln** compounds.

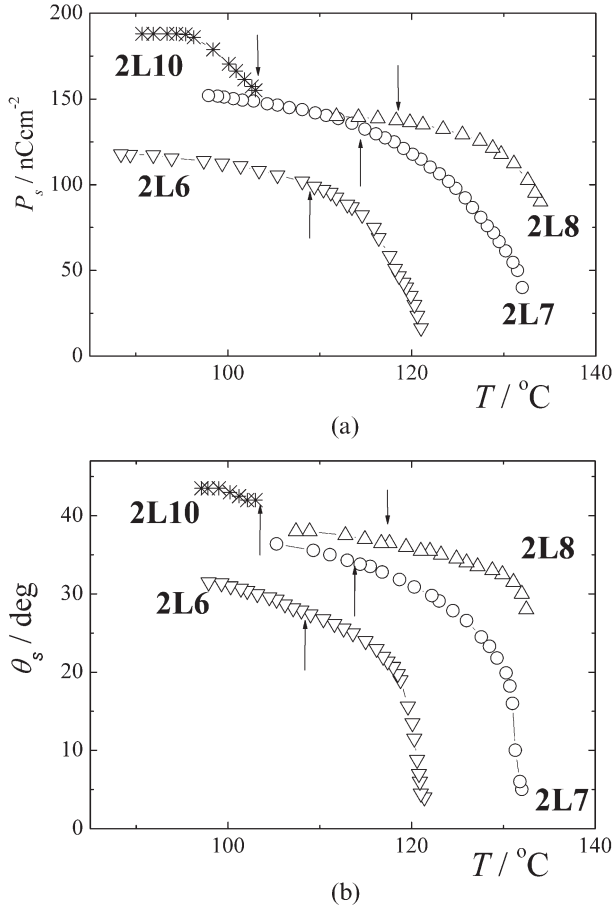

Figure 8. The temperature dependence of (a) the spontaneous polarisation and (b) spontaneous tilt angle for indicated **2Ln** compounds. Arrows indicate the phase transition to the SmC_A* phase.

45° at saturation. The P_s values are typically higher in the **1Ln** series than in **2Ln** homologues. As usual, no anomaly in $P_s(T)$ and $\theta_s(T)$ was found at the transition to the SmC_A* phase.

In order to show the effect of the number of the lactate units, temperature dependences of the spontaneous quantities for compound with three lactate units **3L5** are shown together with those for **1L5** and **2L5** in Figure 9. Besides the substantial decrease of the SmA*–SmC* phase transition temperature with increasing number of lactate units, compounds with one lactate unit reach significantly higher P_s and θ_s values than those with two or three lactate units (see Figures 9a and 9b, respectively).

Dielectric spectroscopy

Frequency dispersions (1 Hz–1 MHz) were fitted to equation (2) and the resulting relaxation frequency and dielectric strength of the detected relaxation modes are shown in Figure 10 and Figure 11 for compounds **1L8** and **2L8**, respectively.

In the paraelectric SmA* phase of **1L8** as well as **1L9** compound, the relaxation frequency of the soft mode linearly decreases and dielectric strength slightly increases when approaching the transition to the SmC* phase. A jump of permittivity when entering the SmC* phase arises due to a strong contribution of the Goldstone mode. A strong increase of the permittivity on cooling within the SmC* phase (see Figure 11) might be caused by an increase of the helical pitch. Such an increase can not be confirmed experimentally as the dechiralisation lines connected with the helix are not seen in the microscope, and thus the pitch is not measurable by a diffraction of the visible light. The reason is that the helical pitch is significantly shorter than 1 μm within the whole temperature range of the SmC* phase. The small value of the pitch was confirmed by applying a

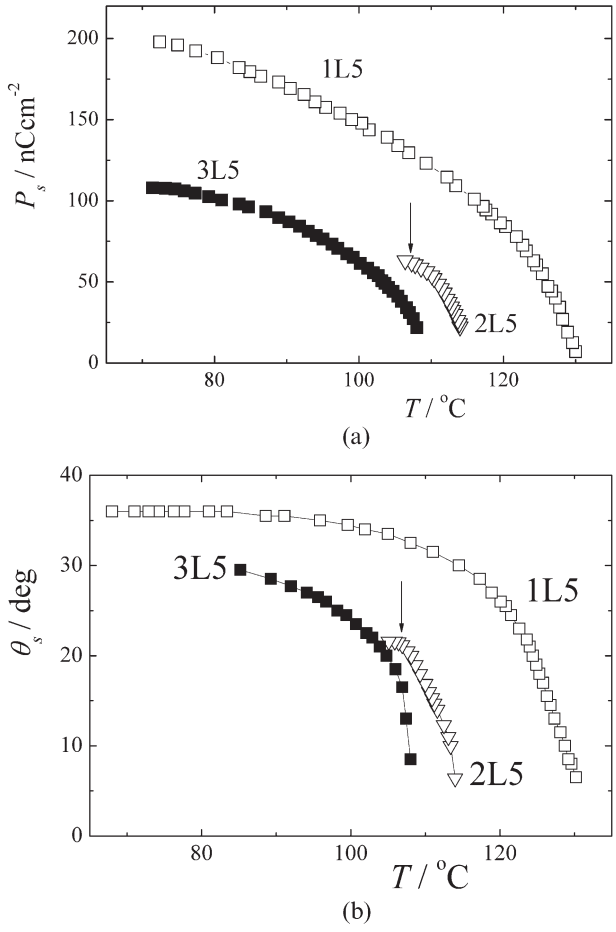

Figure 9. The temperature dependence of (a) the spontaneous polarisation and (b) spontaneous tilt angle for indicated ***x*L5** compounds (x=1, 2, 3). The arrow indicates the phase transition to the SmC_A* phase for **2L5** compound.

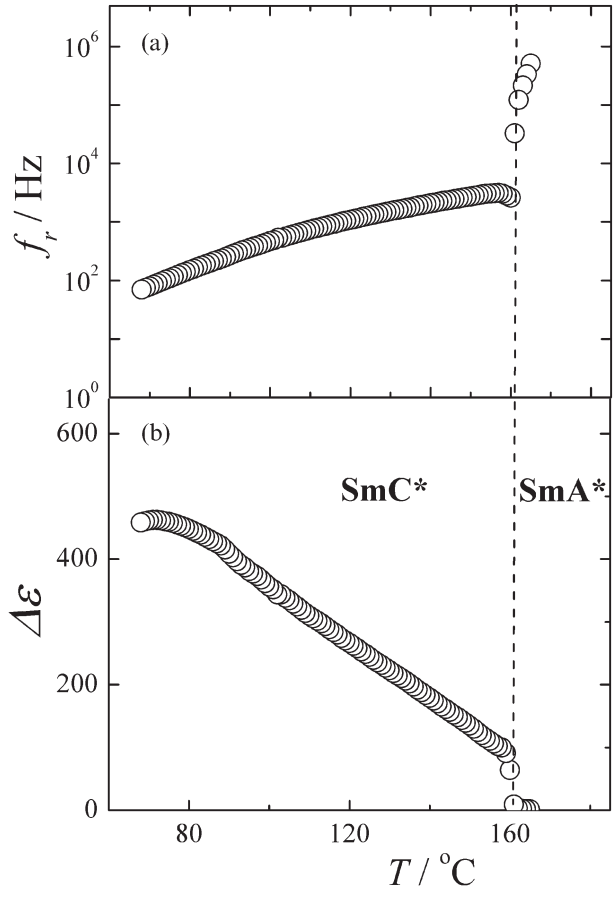

Figure 10. Temperature dependences of (a) the relaxation frequency and (b) the dielectric strength obtained on cooling within the temperature range of the SmA* and SmC* phases for compound **1L8**.

low bias electric field, which causes the prolongation of the pitch and appearance of the dechiralisation lines. Additionally, the selective reflection colours have been observed for free standing films, supporting the fact that the length of the helical pitch is in the wavelength of the visible light range (see above). Slight decrease of the relaxation frequency of the Goldstone mode on cooling (see Figure 11) can be caused also by the pitch length increase and/or by the viscosity increase.

Qualitatively the same results as for **1L8** have been obtained for **1Ln**, n=5–7, where the SmA* phase is replaced by the TGB_A phase. The soft mode has been observed in the whole temperature interval of the TGB_A phase and the typical decrease of the relaxation frequency and increase of the dielectric strength was obtained on cooling to the TGB_A–SmC* phase transition. The Goldstone mode in the SmC* phase of this series exhibits the same features as that shown for **1L8** compound.

For **2Ln** compounds there is a very strong contribution of the Goldstone mode in the SmC* phase similarly to **1Ln** compounds (see figure 11b for **2L8** compound). In the SmC_A* phase two modes have been detected, the relaxation frequencies of both of them, f_h and f_l, decrease on cooling, the value of $\Delta\varepsilon$ being nearly temperature independent. Generally, in the SmC_A* phase and in the frequency range studied here, one can expect the anti-phase mode (*25*) and the rotation of molecules around their short axes, the last being not a collective mode (*26*) and thus exhibiting higher relaxation frequency. The in-phase mode could be active only under a bias field (*27*).

We tested temperature dependences of the relaxation frequencies of both detected modes by the Arrhenius law:

$$f \sim \exp(-E_a/k_BT), \tag{3}$$

where E_a is the activation energy, k_B is the Boltzman constant and T is the temperature. The results are

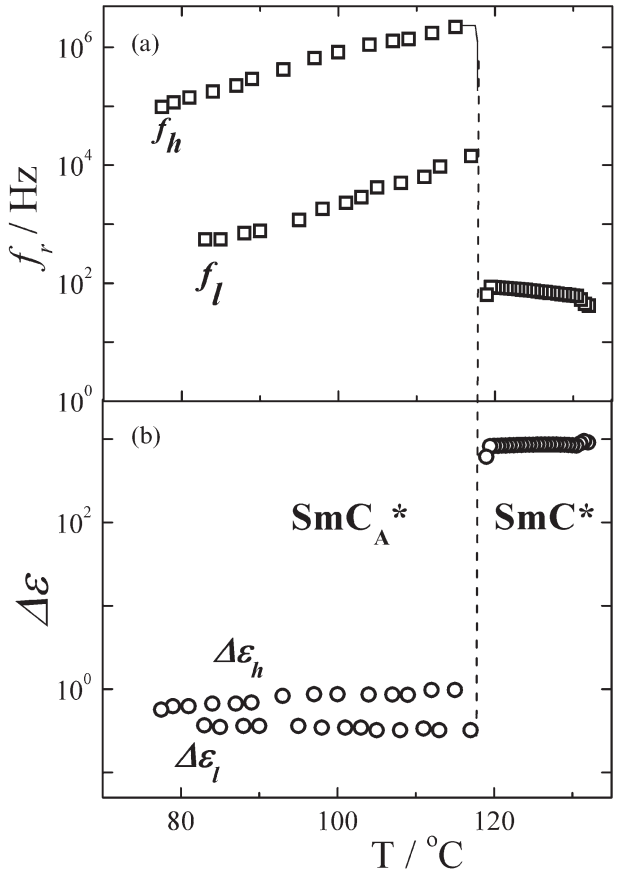

Figure 11. Temperature dependences of (a) the relaxation frequency and (b) dielectric strength obtained on cooling within the temperature range of the SmC* and SmC$_A$* phases for compound **2L8**.

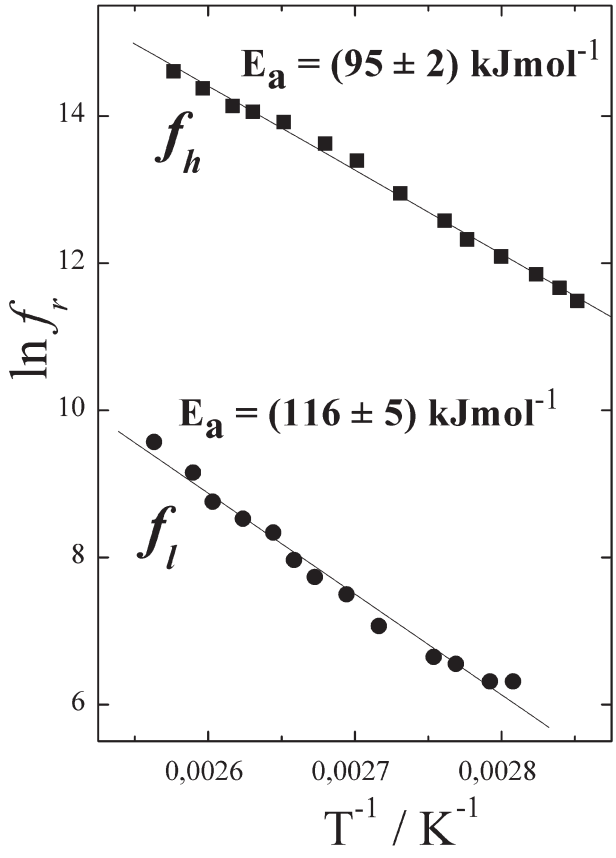

Figure 12. The Arrhenius plot for relaxation frequencies related to the detected modes in the SmC$_A$* phase for compound **2L8**. Fitted values of the activation energy, E_a, for both modes are added.

shown in Figure 12. The temperature dependence of f_h, which is in a good agreement with the Arrhenius equation, can be attributed to the rotation of molecules around their short axes, which exhibits Arrhenius behaviour. The mode with the relaxation frequency f_l can be attributed to the anti-phase mode. The lowering of f_l on cooling, which can be seen in Figures 11 and 12 and which follows the Arrhenius law, might be caused by the viscosity increase.

4. Conclusions

The study of a new series of chiral liquid crystalline materials differing in the number of lactate groups in the chiral part of the molecule provides knowledge on formation of phases in these systems. In general, increasing the number of the lactate groups from one to three results in a decrease of the phase transition temperatures. A similar effect was described previously (*2*) and could be explained by a prolongation of the molecule. All compounds from the **1Ln** series with one lactate group exhibit the ferroelectric SmC* phase and for the shorter homologues up to n=8 the paraelectric SmA* phase, both phases being several tens of degrees broad. For compounds with n=9 and 10, the TGB$_A$ phase is observed and for compounds with n=11 and 12 a direct transition from the isotropic to the ferroelectric SmC* phase takes place.

Introduction of the second lactate group (**2Ln** series) provides broad antiferroelectric SmC$_A$* phase and for compounds with n=5–7 also the SmA* phase. For homologues with n=11–13, a rather rare SmQ phase occurs just below the isotropic phase. X-ray diffraction in this phase shows modulation in two directions and symmetry $I4_122$. Very low birefringence of planar texture (see Figure 3) indicates that model I suggested by Pansu *et al.* (*23*) is quite compatible with the structure of this SmQ phase. In this model, the molecules are tilted compared to the optical (tetragonal) axis and due to the fourfold symmetry the birefringence is expected to be smaller than that in alternative model II, where the molecules are perpendicular to the optical axis.

The behaviour of temperature dependences of the spontaneous tilt angle and spontaneous polarisation

confirm the first-order SmA*–SmC* phase transition for homologues with $n=6$ (see Figures 7 and 8, respectively), the discontinuity being increased with increasing n value. The phase transition from the TGB_A phase to the SmC* phase is strictly of the first order. For all studied compounds, the spontaneous polarisation and tilt angle are high, the values of P_s exceeding $100\,nC\,cm^{-2}$ and the values of θ_s reaching nearly 45° in the longest **1Ln** homologues.

The temperature dependence of the layer spacing reveals a decrease of the layer thickness at the SmA*–SmC* phase transition related to the increased tilt of the molecules. Dielectric spectroscopy reveals the soft mode in the SmA* and TGB_A phases, the Goldstone mode in the SmC* phase and two modes in the SmC_A* phase. In the antiferroelectric phase, the high-frequency mode is attributed to the rotation of molecules around their short axes and the low-frequency mode to the anti-phase mode. The relaxation frequencies of both modes obey the Arrhenius law.

Acknowledgements

This work was supported by the following projects: No. IAA100100710 from the Grant Agency of the Academy of Sciences of the Czech Republic, No. 202/05/0431 from the Czech Science Foundation, AVOZ10100520 of the Academy of Sciences of the Czech Republic, No.OC175 from the Ministry of Education, Youth and Sports of the Czech Republic and bilateral Czech–Polish project No.8 (2006–07).

References

(1) Kašpar M.; Hamplová V.; Novotná V.; Glogarová M.; Pociecha D.; Vaněk P. *Liq. Cryst.* **2001**, *28*, 1203–1211.
(2) Hamplová V.; Bubnov A.; Kašpar M.; Novotná V.; Pociecha D.; Glogarová M. *Liq. Cryst.* **2003**, *30*, 627–631.
(3) Nguyen H.T.; Ismaili M.; Isaert N.; Achard M.F. *J. Mater. Chem.* **2004**, *14*, 1560–1566.
(4) Novotná V.; Glogarová M.; Hamplová V.; Kašpar M. *J. Chem. Phys.* **2001**, *115*, 9036–9041.
(5) Hamplová V.; Kašpar M.; Novotná V.; Glogarová M. *Ferroelectrics* **2002**, *276*, 45–54.
(6) Kašpar M.; Górecká E.; Sverenyák H.; Hamplová V.; Glogarová M.; Pakhomov S.A. *Liq. Cryst.* **1995**, *19*, 589–594.
(7) Bubnov A.; Hamplová V.; Kašpar M.; Glogarová M.; Vaněk P. *Ferroelectrics* **2000**, *243*, 27–35.
(8) Meier J.G.; Rudquist P.; Petrenko A.S.; Goodby J.W.; Lagerwall S.T. *Liq. Cryst.* **2002**, *29*, 179–189.
(9) Nishiyama I.; Yamamoto J.; Goodby J.V.; Yokoyama H. *J. Mater. Chem.* **2002**, *12*, 1709–1716.
(10) Demikhov E.; Stegmeyer H. *Liq. Cryst.* **1991**, *10*, 869–873.
(11) H.-S Kitzwerow. *Chirality in Liquid Crystals,* Springer-Verlag, New York 2001. 296–346.
(12) Renn S.R.; Lubensky T.C. *Phys. Rev. A* **1998**, *38*, 2132–2147.
(13) Renn S.R. *Phys. Rev. A* **1992**, *45*, 953–973.
(14) Goodby J.W.; Waugh M.A.; Stein S.M.; Chin E.; Pindak R.; Patel J.S. *Nature* **1989**, *337*, 449–452.
(15) Goodby J.W.; Waugh M.A.; Stein S.M.; Chin E.; Pindak R.; Patel J.S. *J. Am. Chem. Soc.* **1989**, *111*, 8119–8125.
(16) Goodby J.W.; Slaney A.J.; Booth C.J.; Nishiyama I.; Vuijk J.D.; Styring P.; Toyne K. *Mol. Cryst. Liq. Cryst.* **1994**, *243*, 231–298.
(17) Bennemann D.; Heppke G.; Levelut A.M.; Lötzsch D. *Mol. Cryst. Liq. Cryst.* **1995**, *260*, 351–360.
(18) Levelut M.; Germain C.; Keller P.; Liebert L.; Billard J. *J. Phys., Paris* **1983**, *44*, 61–66.
(19) Levelut M.; Hallouin E.; Bennemann D.; Heppke G.; Lötzsch D. *J. Phys., Paris II* **1997**, *7*, 981–1000.
(20) Levelut M.; Bennemann D.; Heppke G.; Lötzsch D. *Mol. Cryst. Liq. Cryst.* **1997**, *299*, 433–438.
(21) Takanishi Y.; Takezoe H.; Yoshizawa A.; Kusumoto T.; Hyiama T. *Mol. Cryst. Liq. Cryst.* **2000**, *347*, 501–508.
(22) Kusumoto T.; Sato K.; Katoh M.; Matsutani H.; Yoshizawa A.; Ise N.; Umezawa J.; Takanishi Y.; Takezoe H.; Hyiama T. *Mol. Cryst. Liq. Cryst.* **1999**, *330*, 1471–1478.
(23) Pansu B.; Nastishin Y.; Impéror-Clerc M.; Veber M.; Nguyen H.T. *Eur. Phys. J. E* **2004**, *15*, 225–230.
(24) Dierking I., *Textures of Liquid Crystals*; Wiley-VCH Verlag: 2003.
(25) Ikeda A.; Takanishi Y.; Takezoe H.; Fukuda A. *Jap. J. Appl. Phys.* **1993**, *32*, L97–L100.
(26) Wrobel S.; Haase W.; Fafara A.; Marzec M. *Relaxation Phenomena*; Springer: 2003.
(27) Parry-Jones L.A.; Elton S.J. *Phys. Rev. E* **2001**, *63*, 050701 (1–4).